

Gasdermin D inhibition confers antineutrophil mediated cardioprotection in acute myocardial infarction

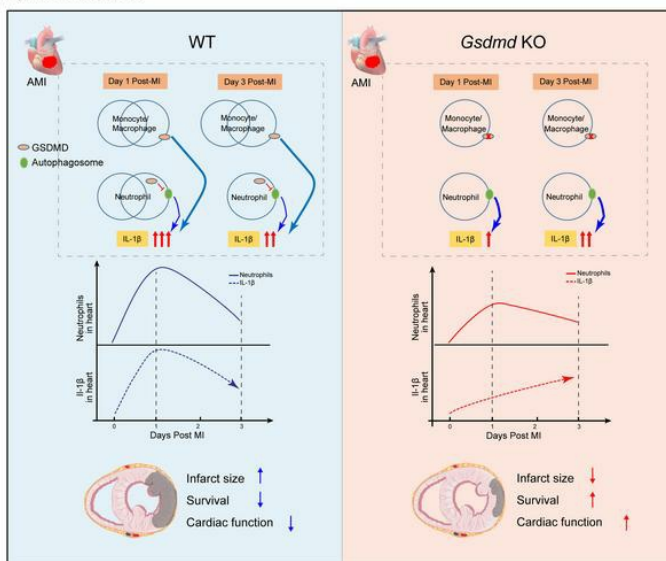
Kai Jiang, ... , Dandan Wang, Yaozu Xiang

J Clin Invest. 2021. <https://doi.org/10.1172/JCI151268>.

Research In-Press Preview Cardiology

Graphical abstract

Graphical abstract



Find the latest version:

<https://jci.me/151268/pdf>



1 **Title: Gasdermin D inhibition confers antineutrophil mediated cardioprotection in acute**
2 **myocardial infarction**

3 **Authors:**

4 Kai Jiang^{1#}, Zizhuo Tu^{1#}, Kun Chen^{1#}, Yue Xu¹, Feng Chen¹, Sheng Xu², Tingting Shi², Jie Qian¹,
5 Lan Shen³, John Hwa⁴, Dandan Wang¹, Yaozu Xiang^{1, 2*}

6 **Affiliations:**

7 ¹Shanghai East Hospital, Key Laboratory of Arrhythmias of the Ministry of Education of China,
8 School of Life Sciences and Technology, Tongji University; Shanghai, 200092, China.

9 ²Shanghai Tenth People's Hospital, Tongji University School of Medicine; Shanghai, 200072,
10 China.

11 ³Department of Cardiology, Clinical Research Unit, Shanghai Chest Hospital, Shanghai JiaoTong
12 University, 241 Huaihai West Rd, Shanghai 200030, China

13 ⁴Section of Cardiovascular Medicine, Department of Internal Medicine, Yale Cardiovascular
14 Research Center, Yale University School of Medicine, New Haven, CT, 06511 USA

15

16 ***Corresponding:**

17 Yaozu Xiang, MD, PhD

18 Shanghai East Hospital, School of Life Sciences and Technology, Tongji University,

19 Shanghai, 200092, China. Email: yaozu.xiang@tongji.edu.cn

20 [#]These authors contributed equally to this work

21 The authors have declared that no conflict of interest exists.

22

23 **Abstract**

24 Acute myocardial infarction (AMI) induces blood leukocytosis, which correlates inversely with
25 patient survival. The molecular mechanisms leading to leukocytosis in the infarcted heart, remain
26 poorly understood. Using an AMI mouse model, we identified gasdermin D (GSDMD) in activated
27 leukocytes early in AMI. We demonstrated that GSDMD is required for enhanced early
28 mobilization of neutrophils to the infarcted heart. Loss of GSDMD resulted in attenuated IL-1 β
29 release from neutrophils and subsequent decreased neutrophils and monocytes in the infarcted
30 heart. Knockout of GSDMD in mice significantly reduced infarct size, improved cardiac function,
31 and increased survival post AMI. Through a series of bone marrow transplantation studies and
32 leukocytes depletion experiments, we further clarified that excessive bone marrow derived and
33 GSDMD-dependent early neutrophil production and mobilization (24 hours post AMI),
34 contributed to the detrimental immunopathology after AMI. Pharmacological inhibition of
35 GSDMD also conferred cardioprotection post AMI, through reduction of scar size and
36 enhancement of heart function. Our study provides new mechanistic insights into molecular
37 regulation of neutrophil generation and mobilization after AMI, and supports GSDMD as a new
38 target for improved ventricular remodeling and reduced heart failure after AMI.

39

40

41 **Introduction**

42 Acute myocardial infarction (AMI) is a leading cause of death worldwide. Although reperfusion
43 is successful in reducing infarct size and improving overall prognosis, AMI remains a major cause
44 of heart failure and increased morbidity and mortality (1). In the past two decades, an increasing
45 number of programmed cardiomyocyte cell death have been recognized in AMI and ischemia–
46 reperfusion injury (1, 2). Sudden massive loss of cardiomyocytes post AMI exceeds the limited
47 regenerative capacity of the myocardium (3). Cytokines released from necrotic cells can activate
48 innate immune pathways, triggering an intense inflammatory response (4). Dysregulation of the
49 inflammatory response may cause adverse remodeling (fibrosis and scar formation) in patients
50 with AMI contributing to post infarction heart failure (5). Therapeutic attempts to suppress
51 inflammation during AMI can lead to impaired cardiac repair and increased risk of cardiac rupture
52 (6). More recent strategies aimed at selectively blocking key inflammatory factors rather than
53 globally suppressing the response have shown some promising results (7).

54 Accumulating evidence has underscored a central role of inflammasome in AMI (8). The most
55 widely characterized inflammasome sensor in the heart is the NACHT, LRR, and PYD domains-
56 containing protein 3 (NLRP3), which is activated in response to cell debris during AMI (8).
57 Activation of NLRP3 inflammasome triggers myocardial damage through promotion of
58 inflammatory cell death via pyroptosis and through release of interleukin-1 β (IL-1 β) (8). In
59 contrast, downregulation or inhibition of inflammasome components including Nlrp3 (9), ASC
60 and Casp1 may reduce infarct size (8, 10). However, inhibition of IL-1 β activity appears not to
61 reduce infarct size (11). The pyroptotic substrate is the pore-forming protein gasdermin D
62 (GSDMD) (12-14), which is widely expressed in different subsets of leukocytes (15). Cardiac
63 neutrophil and monocyte/macrophage numbers expand rapidly in the days following AMI (16).

64 Recent findings suggests that GSDMD plays a distinct role in neutrophils during inflammasome
65 activation, which differs from its role in macrophages (17, 18). The regulatory role of GSDMD in
66 response to AMI is unknown.

67 We now demonstrate that GSDMD is activated early in AMI and plays a critical role in increased
68 production and mobilization of neutrophils. Both genetic deletion and pharmacological inhibition
69 of GSDMD attenuated myocardial injury, reduced infarct size and improved cardiac function and
70 survival. We further demonstrated that GSDMD deficiency reduced acute cardiac cell death and
71 IL-1 β production independent of NLRP3 inflammasome activation. Consequently, reduced
72 leukocyte numbers in the blood (and infarct) decreased inflammation and diminished post-AMI
73 heart failure. Our work thus identifies GSDMD-dependent, bone marrow derived neutrophil
74 generation and mobilization, as an important contributing factor to cardiac immunopathology after
75 AMI, and provides mechanistic insights into modulation of inflammatory response during AMI,
76 involving pyroptosis-dependent and pyroptosis -independent regulatory networks.

77

78 **Results**

79 ***GSDMD is activated in the early phase of AMI***

80 We initially examined transcription levels of key factors involved in the acute inflammatory
81 response to AMI by RNA sequencing of murine heart samples post AMI. Hierarchical clustering
82 demonstrated samples from different experimental groups (sham, 1-day and 1-week post AMI
83 groups) to be well separated from each other, while biological replicates from the same group
84 clustered together well (**Supplemental Figure 1A**). We found 204 genes significantly up-
85 regulated on Day1 AMI samples compared to the Sham samples and Day 7 AMI samples, while

86 64 genes were significantly downregulated (**Figure 1A**). Differentially expressed genes that had
87 consistent expression patterns across Sham, AMI (Day 1) and AMI (Day 7) were further clustered
88 together, and genes encoding the components of inflammasome showed a distinct increase,
89 indicating the inflammasome may be activated post AMI (**Figure 1, B and C, and Supplemental**
90 **Figure 1**). Furthermore, “Biological Process” enrichment analysis of DEGs also suggested
91 upregulation of inflammatory responses, including “neutrophil chemotaxis”, and “cellular
92 response to Il-1” (**Supplemental Figure 1C**). Interestingly, *Nlrp3*, encoding a pattern recognition
93 receptor, was rapidly upregulated within 24 hours post AMI followed by decline in expression at
94 day 7 post AMI (**Figure 1C**). The expression of the downstream components of NLRP3 activation
95 including *Casp1*, *Gsdmd*, *Il1b*, was upregulated in response to AMI, indicating myocardial NLRP3
96 inflammasome could be activated during AMI (**Figure 1C**). We further validated these findings
97 by evaluating the protein level and activation level of *Gsdmd* in the heart. Baseline GSDMD
98 exhibited low level of expression in heart but high level in other tissues like intestine, liver and
99 spleen (**Figure 1D**), consistent with previous reports that GSDMD exhibited high level in
100 immunocytes and fibroblasts and low level in cardiomyocytes, endothelial cells and smooth
101 muscle cells (19, 20). Intriguingly, both expression and activation of GSDMD in heart were
102 remarkably enhanced in response to myocardial ischemia/infarction in left anterior descending
103 (LAD) ligation-operated wild type (WT) mice, as early as 24 hours post AMI (**Figure 1, E and**
104 **F**). In addition, NLRP3, Caspase-1 cleavage and particularly Il-1 β were induced early during
105 myocardial ischemia/infarction (**Figure 1, E and F**). Taken together, these data suggest NLRP3
106 inflammasome and GSDMD-induced pyroptosis may be activated early post AMI and the likely
107 source is from infiltrating leukocytes.

108

109 ***Loss of GSDMD attenuates myocardial injury post AMI***

110 To determine the overall role of GSDMD in acute AMI, we initially utilized *Gsdmd*^{-/-} (global
111 knockout) mice and subjected the hearts to sham operations or AMI (as will be described later
112 bone marrow transplantation and leukocyte depletion studies will provide tissue specific knockout
113 studies). Unexpectedly, we observed significantly improved survival of the *Gsdmd*^{-/-} mice post
114 AMI compared with AMI-operated WT littermate controls (78.7% versus 50%, *P* = 0.0108)
115 (**Figure 2A**). *Gsdmd* deficiency appeared to significantly improve left ventricular systolic function,
116 which was severely impaired following AMI in WT littermate controls (**Figure 2, B and C**).
117 Consistently, the ratio of heart weight to body weight ratio in *Gsdmd*^{-/-} mice was significantly
118 decreased compared to that of the littermate controls (**Figure 2D**). We further determined the effect
119 of *Gsdmd* deficiency on cardiac structural remodeling post AMI. Masson's Trichrome staining
120 analysis and quantification of the scar showed that the hearts from *Gsdmd*^{-/-} mice had significant
121 reduction in fibrotic scar size (**Figure 2, E and F**) and increase in thickness of left ventricular (LV)
122 wall (**Figure 2F**). Apart from utilizing LAD ligation-operated mice, we also compared the
123 myocardial infarction size in response to ischemia (30 minutes)/ reperfusion (24 hour) (I/R) in
124 mice (**Figure 2G**). Remarkably, we observed that *Gsdmd*^{-/-} mice compared to that of the littermate
125 controls also exhibited a significant reduction in infarct size (**Figure 2, H and I**). These data
126 suggested that *Gsdmd* deficiency reduces infarct size, preserves cardiac function, and improves
127 survival post AMI. We set forth to determine the mechanisms for this unexpected protective effect.

128

129 ***GSDMD is essential for recruitment of neutrophils/monocytes to the infarcted heart***

130 To explore the mechanisms underlying GSDMD deficiency conferred cardioprotection post AMI,
131 and based upon recent suggestions that GSDMD may play a role in neutrophil
132 production/mobilization, we investigated leukocyte infiltration and leukocytosis in AMI
133 **(Supplemental Figure 2)**. After AMI, an increase particularly in neutrophils (and to a lesser extent
134 monocyte) recruitment to the infarcted heart occurred within 12 hours, peaking at 24 hours
135 (neutrophil) and 72 hours (monocyte) respectively during the 3-day observation period **(Figure 3,**
136 **A and B)**. The number of neutrophils (and monocytes) in the blood exhibited a similar pattern,
137 with neutrophils peaking at 12 hours **(Figure 3, C and D)**. This initial surge in blood neutrophils
138 might result from mass exodus of neutrophils from the hematopoietic stem and progenitor cells in
139 the bone marrow **(Figure 3, E and F)**. Consistent with this notion, there was an initial significant
140 decrease in the overall number of neutrophils (and monocytes) in the bone marrow followed by an
141 increase in numbers **(Figure 3, E and F)**, supporting the majority of the initial neutrophil
142 mobilization as being from the bone marrow followed by new production of neutrophils, consistent
143 with previous reports (16). Furthermore, in *Gsdmd*^{-/-} mice, the observed increase in WT was
144 significantly reduced in the heart, blood and bone marrow 24 hours post AMI **(Figure 3, G-J)**,
145 supporting an important role for GSDMD in neutrophil generation and mobilization in AMI.
146 Intriguingly, there was no difference in number of neutrophils in the heart, blood and bone marrow
147 between WT and *Gsdmd*^{-/-} mice 72 hours post AMI **(Figure 4, A and B)**. In contrast, *Gsdmd*^{-/-}
148 mice exhibited a marked reduction in number of monocytes both in heart and blood 72 hours post
149 AMI compared to WT mice **(Figure 4, A and B)**. These suggest that the inhibition of GSDMD
150 could apply a brake on neutrophil mobilization at the initial stages of the inflammatory response
151 to an AMI.

152 To validate these findings, we further sectioned the infarcted heart followed by
153 immunofluorescence staining with MPO or CD68 antibody to specifically label and visualize the
154 local neutrophils (MPO) and monocytes/macrophages (CD68⁺). At 24 hours post AMI, in the WT
155 mice a large number of MPO⁺ neutrophils were recruited to the infarcted heart, while the number
156 of neutrophils in the infarcted heart of *Gsdmd*^{-/-} mice were markedly reduced (**Figure 4, C and**
157 **D**). Notably, there was no difference in the number of the TUNEL-positive apoptotic cells in the
158 infarcted heart between *Gsdmd*^{-/-} mice and controls (**Figure 4, C and E**), suggesting that GSDMD
159 deletion did not affect cardiac apoptosis after AMI, consistent with its key specific role in
160 pyroptosis. By the end of the 72 hours post AMI, a large number of monocytes/macrophages were
161 also recruited into both infarct zone and border zone of the heart in WT mice (**Figure 4, G-H**).
162 Again, the *Gsdmd*^{-/-} mice showed a significant decrease in the monocytes/macrophages infiltration
163 particularly in the infarct border zone (**Figure 4, E and H**), suggesting the critical role of GSDMD
164 in mediating function of monocytes/macrophages in the later acute phase of an AMI. Together,
165 the data supports that GSDMD is involved in the recruitment of neutrophils (and monocytes) to
166 the infarcted heart, contributing to the inflammatory response.

167 In addition, similar patterns of neutrophil and monocyte counts was observed in response to
168 myocardial I/R (**Figure 5, A-F**). Notably, that *Gsdmd* deletion did not affect baseline leukocyte
169 proportion (**Supplemental Figure 3**). Collectively, observation of significant reduction in the
170 mobilized neutrophils in the heart 24 hours post AMI (**Figure 3, G-J**) and I/R (**Figure 5, G and**
171 **H**) in *Gsdmd*^{-/-} mice, suggests a distinct role of GSDMD in regulating neutrophils in response to
172 AMI.

173 ***GSDMD deficiency reduces cell death and IL-1 β***

174 As noted above there was no difference in TUNEL positive apoptotic cell death between the WT
175 and *Gsdmd*^{-/-} mice. AMI-induced activation of NLRP3 inflammasome triggers further myocardial
176 damage indirectly through the release of IL-1 β and directly through promotion of inflammatory
177 cell death via pyroptosis (8). Given GSDMD's role in releasing IL-1 β from neutrophils
178 independent of pore formation (18), we next sought to explore possible mechanisms for reduced
179 recruitment of neutrophils to the infarcted heart caused by GSDMD deficiency. To determine
180 secretion of IL-1 β from leukocytes in the infarcted heart, CD11b⁺ leukocytes or Ly6G⁺ neutrophils
181 were isolated from sham and ischemic mouse hearts (*Gsdmd*^{-/-} mice and littermate controls), as
182 described previously (21). The isolated CD11b⁺ or Ly6G⁺ neutrophils were cultured for 24 hours,
183 followed by assays to measure the LDH, IL-1 β , IL-18 and MCP-1 level (**Figure 6A and**
184 **Supplemental Figure 4, A and B**). We observed significant reduction in both LDH and IL-1 β
185 level in isolated CD11b⁺ leukocytes from *Gsdmd*^{-/-} mice compared to those from littermate
186 controls after AMI-24h, with no significant difference 72h post-AMI (**Figure 6, B and C**). In
187 contrast, there was no significant difference in both IL-1 β and LDH level in isolated neutrophils
188 from *Gsdmd*^{-/-} mice and WT mice after AMI-24h, but a significant increase in IL-1 β level in
189 *Gsdmd*^{-/-} mice 72h post-AMI (**Figure 6, D and E and Supplemental Figure 4, C and D**).
190 Consistently, serum LDH level was markedly elevated 24 hours post AMI in WT mice while
191 significantly reduced in *Gsdmd*^{-/-} mice (**Supplemental Figure 4E**). However, serum IL-1 β
192 showed an equal level between WT mice and *Gsdmd*^{-/-} mice 72 hours post AMI (**Supplemental**
193 **Figure 4F**). These suggest that it is neutrophil-released IL-1 β dominates the serum IL-1 β level 72
194 hours post AMI.

195 To explore how GSDMD modulate neutrophils death and IL-1 β release independent of plasma
196 membrane GSDMD pores and pyroptosis, we further analyzed the isolated heart and leukocytes

197 samples from *Gsdmd*^{-/-} mice compared to those from littermate controls after AMI-24h and AMI-
198 72h. Although there was no significant difference in NLRP3 activation and cleavage of Caspase-
199 1 and IL-1β in heart 24 hours post AMI between WT mice and *Gsdmd*^{-/-} mice (**Figure 6, F and**
200 **G**), the cleaved LC3 (autophagy marker) in CD11b⁺ leukocytes or Ly6G⁺ neutrophils samples from
201 the *Gsdmd*^{-/-} mice 72 hours post AMI was significantly increased comparable with those in the
202 WT mice (**Figure 6, H and I and Supplemental Figure 4, G-I**). These indicated the autophagic
203 flux in neutrophils may be enhanced by GSDMD deficiency, contributing to the release of IL-1β
204 from neutrophils. Taken together, these data suggest that AMI-mediated activation of GSDMD
205 resulting in the release of IL-1β, possibly leading to cardiac inflammation by recruitment of
206 neutrophils to the infarcted heart.

207

208 ***GSDMD-dependent bone marrow-derived myeloid cell contributes to acute inflammatory***
209 ***response***

210 Given that release of IL-1β induced by myocardial injury can be from leukocytes and non-
211 leukocytes (e.g., fibroblast) (10), we hypothesized that AMI-induced neutrophil infiltration
212 requires the GSDMD activation in cardiac neutrophils. To test this hypothesis, we transplanted
213 bone marrows from WT or *Gsdmd*^{-/-} mice into WT mice, or bone marrow from WT into *Gsdmd*^{-/-}
214 mice, and then subjected the transplanted animals to AMI (**Figure 7A and Supplemental Figure**
215 **5A**). This serves as a bone marrow specific knockout of *Gsdmd*. Consistent with our proposed
216 sequelae of events, AMI-induced poor survival and adverse cardiac remodeling was improved by
217 *Gsdmd*^{-/-} bone marrow transplantation (**Figure 7, B-D**). There was no difference in cardiac
218 function 1 week post MI among those that survived (**Supplemental Figure 5, B-F**). Given that

219 transplantation of wild-type bone marrow into *Gsdmd*^{-/-} mice did not fully restore the WT
220 phenotype (**Figure 7B**), a number of explanations are possible including gasdermin D in some not-
221 radiosensitive cell may also contribute.

222 To further characterize the role of neutrophils in contributing to myocardial injury in vivo, we next
223 depleted neutrophils or neutrophils/monocytes by intraperitoneal injection of anti-Ly6G and anti-
224 Ly6G/Ly6C antibodies, respectively (**Figure 7E**). Injection of anti-Ly6G antibody effectively
225 depleted the circulating neutrophils and did not affect the number of monocytes (**Figure 7F and**
226 **Supplemental Figure 6**). Furthermore, anti-Ly6G/Ly6C injection leads to an effective clearance
227 of circulating neutrophils and monocytes (**Figure 7F**). Both mice with neutrophils-depletion and
228 neutrophil/monocyte-clearance exhibited a significantly reduced infarct size compared to control
229 mice (**Figure 7, G and H**). Importantly, there was no significant difference in infarct size between
230 anti-Ly6G injected mice and anti-Ly6G/Ly6C injected mice 72 hours post AMI (**Figure 7H**),
231 which emphasized the critical role of neutrophils in promoting myocardial injury. However,
232 depletion of neutrophils with anti-Ly6G for 1 week mildly increased infarct size post AMI (**Figure**
233 **7, I and J**). This key result has important therapeutic implications, suggesting neutrophil depletion
234 should be short term (first 3 days) as longer-term depletion (1 week) can be detrimental. These
235 data suggest that bone marrow-derived neutrophils contribute to acute inflammatory response to
236 AMI and their conferred cardioprotection depends on GSDMD activity.

237

238 *Pharmacological inhibition of GSDMD reduces infarct size post AMI*

239 The bone marrow transplant data suggests that GSDMD inhibition reduces infarct size and
240 preserves cardiac function through leukocyte suppression. Given that pyroptotic cell death can be

241 pharmacologically inhibited by necrosulfonamide (NSA) (22), the role of NSA as a therapy in the
242 initial inflammatory response was then tested in vivo in the above mouse model of permanent
243 ligation of the LAD (**Figure 8A and Supplemental Figure 7A**). We optimized the dosage of NSA
244 for in vivo stability, according to previous reports (22), and found that NSA administration with a
245 dose of 20 mg/kg either 30 minutes before LAD ligation (**Figure 8**) or within 30 minutes (DMSO:
246 11.3 ± 1.9 min; NSA 11.2 ± 2.2 min) post LAD ligation (**Supplemental Figure 7**) did not
247 demonstrate any adverse short term survival effect (toxicity or arrhythmia) one week post AMI
248 (**Figure 8B and Supplemental Figure 7B**). However, there was significant improvement in
249 systolic function (**Figure 8, C and D, and Supplemental Figure 7, C and D**). Masson's Trichrome
250 staining analysis of the scar showed that NSA treatment significantly reduced the fibrotic scar size
251 (**Figure 8E and Supplemental Figure 7, E and F**) and increased LV wall thickness (**Figure 8F**).
252 On the basis of our findings from the murine AMI models, GSDMD inhibition (within hours of
253 AMI) may be a novel therapy to reduce scar formation and prevent heart failure post AMI.
254 Inhibition of excess early (1-3 days) leukocyte mobilization and myocardial leukocyte infiltration
255 may also be a potential strategy for therapy of AMI.

256

257 *Human studies confirm the importance of AMI associated neutrophilia.*

258 To highlight the impact of post AMI neutrophilia in human subjects we recruited 234 patients who
259 had an AMI with only a single left anterior descending branch blockage (analogous to our mouse
260 LAD ligation model) (**Supplemental Table1**) and correlated their neutrophil percentage to
261 ejection fraction 5 days post PCI. There was a clear statistical negative correlation ($R=-0.41$,
262 $p<0.0001$) (**Figure 8G**), with increased neutrophil percentage (greater than 60% being neutrophilia)

263 being associated with a reduced ejection fraction. In contrast, there was no significant correlation
264 between monocytes (both admission and within 24 hours post PCI) and ejection fraction within 5
265 days post PCI. Taken together our mice AMI studies in combination with our preliminary human
266 studies highlight the potential benefits of GSDMD inhibition in improving ventricular function
267 and survival post AMI.

268

269 **Discussion**

270 Despite significant advances in percutaneous and surgical reperfusion, many patients who have an
271 AMI ultimately develop heart failure with its associated poor prognosis. New mechanism-based
272 therapies are urgently needed. An intense inflammatory response is triggered after myocardial
273 ischemia and necrosis (23). Inflammation, although essential for wound healing, can mediate
274 excessive scar formation and dysfunctional ventricular remodeling (24, 25). Clinically,
275 neutrophilia (a key component of the inflammatory response to AMI) correlates with major
276 adverse cardiovascular events in patients with AMI (16), implying neutrophil reduction may have
277 more favorable outcomes. However, the mechanisms that determine neutrophil generation and
278 recruitment to the infarcted heart remain unclear. Herein, we report that AMI-induced neutrophilia
279 and early neutrophil infiltration into the heart are linked to increased expression and activation of
280 inflammasome-effector GSDMD. Global knockout of *Gsdmd*, bone marrow-specific knockout of
281 *Gsdmd* by BMT, and chemical inhibition of GSDMD reduced infarct size and improved cardiac
282 function post AMI. In addition, GSDMD deficiency attenuated the myocardial injury in a murine
283 ischemia reperfusion model. Loss of GSDMD resulted in decreased early generation and
284 mobilization of neutrophils and monocytes to the infarcted heart. Furthermore, clearance of

285 neutrophils in vivo improved the heart function post AMI. Taken together, our findings support
286 that inhibition of early neutrophil generation and mobilization is cardioprotective for AMI.

287

288 Cardiac neutrophils are the first responder in amplifying the acute inflammatory response after
289 AMI. The initial wave of infiltrating neutrophils sets the tone for the ensuing inflammatory
290 response by releasing key factors that activate the NLRP3 inflammasome, and promote the
291 secretion of IL-1 β (7). The released IL-1 β interacts with interleukin 1 receptor type 1 on myeloid
292 progenitor cells in the bone marrow and stimulates granulopoiesis in a cell-autonomous manner.
293 Genetic deletion or pharmacological inhibition of the NLRP3 inflammasome–IL-1 β signaling axis
294 dampens granulopoiesis and improve cardiac function in mouse models of AMI (8). Although
295 GSDMD promotes IL-1 β release from hyperactive macrophages (26) and targeting IL-1 β reduces
296 leukocyte production after AMI (7, 11), how the release of IL-1 β from distinct subsets of
297 leukocytes and non-leukocytes is regulated in response to AMI is not fully understood. Our study
298 demonstrated that GSDMD was predominantly expressed in leukocytes, but not in other types of
299 cells in the heart tissue (data not shown). Importantly, through bone marrow transplantation, we
300 demonstrated GSDMD-dependent neutrophil recruitment was required for myocardial injury in
301 early phase. GSDMD deficiency reduced release of IL-1 β from neutrophils and acute
302 inflammatory response post AMI. For clinical translation, we further tested the inhibitor of
303 pyroptotic cell death, NSA, which has recently been reported to inhibit GSDMD-mediated pore
304 formation in cell membrane and subsequent pyroptosis (22), in a murine AMI model. We
305 demonstrated that pharmacological inhibition of GSDMD also conferred cardioprotection post
306 AMI, in reducing scar size and enhancing heart function. Although there is no difference in
307 survival, significantly increased ejection fraction would be clinically associated with improved

308 signs and symptoms of heart failure, improved exercise tolerance, as well as reduced
309 hospitalizations. With an increased cohort of treated mice, as well as longer term follow-up, we
310 anticipate the significantly improved ejection fraction will translate to increased survival. These
311 findings highlight the potential therapeutic application for targeting GSDMD early after AMI.

312 There has been a contradictory study that neutrophil depletion has no effect on infarct size at 24
313 hours post AMI and progressively worsens cardiac function from day 7 to day 14 (27). Since
314 neutrophils are necessary in the repair process, optimized the dosage and time of anti-Ly6G
315 injection is essential in addition to other supportive genetic, neutrophil depletion, and bone marrow
316 transplant data. This suggests the timing of interventional strategies for targeting GSDMD as well
317 as the degree of neutrophil inhibition are critical in preventing post-infarction heart failure.
318 Previous in vitro studies demonstrated that in the absence of the pyroptosis-mediating substrate
319 GSDMD, caspase-1 activates caspase-3 and induces apoptosis (28), indicating a possible
320 bidirectional crosstalk between apoptosis and pyroptosis in monocytes and macrophages (29).
321 However, in the present study, in vivo analysis with western blot and TUNEL staining revealed
322 that loss of GSDMD did not significantly change the overall level of apoptosis in the infarcted
323 heart (**Figure 4, C and F**). One recent in vitro study using ATG7-deficient cells demonstrated that
324 neutrophils secrete IL-1 β through N-terminal of GSDMD trafficking to neutrophil organelles, an
325 autophagy-dependent mechanism (18), consistent with our findings that GSDMD regulating IL-
326 1 β release independently of plasma membrane pores and pyroptosis in neutrophil. In contrast, we
327 have now demonstrated that GSDMD deficiency triggered autophagic flux in neutrophils using *ex*
328 *vivo* assays (**Figure 6, H and I and Supplemental Figure 4**). This will require further detailed
329 exploration.

330 There are several limitations to this study, including choice of the infarct model. To establish the
331 infarct model, we applied permanent ligation of a normal coronary artery, which differs
332 substantially from the process of atherothrombosis in human subjects. To overcome these
333 limitation, further clinical proof of concept studies that targeting GSDMD and neutrophil
334 generation for management of AMI heart failure are needed.

335 In summary, we found that genetic knockout or pharmacological inhibition of GSDMD
336 significantly improved heart function post AMI. Furthermore, bone marrow transplantation from
337 *Gsdmd* knockout mice show the same improvement. We provide new mechanistic insights into
338 molecular regulation of inflammatory response during an AMI. It is bone marrow derived and
339 GSDMD-dependent neutrophils generation and mobilization that contribute to the detrimental
340 immunopathology after AMI. We anticipate that our studies may be broadly applicable to
341 cardioprotective therapy, specifically targeting GSDMD and neutrophil production for improved
342 ventricular remodeling and reduced heart failure after AMI.

343

344 **Methods**

345 **Human studies**

346 **Study design:** The STEMI follow-up registry was a prospective, longitudinal, multicenter registry
347 study of patients hospitalized with first-time STEMI in east China (ChiCTR-IDR-16007765). The
348 study was performed following the principles of the Declaration of Helsinki. It was approved
349 centrally by the Ethics Committee at Shanghai Chest Hospital, Shanghai Jiaotong University (in
350 Dec. 2015; approved number 2015-111) and by the local health research ethics board at each
351 participating hospital. Written informed consent was obtained from each patient to allow for

352 follow-up data. All data on patient demographics, signs and symptoms, medication, clinical
353 characteristics, and discharge information were collected on a clinical-based registry.

354 **Study population:** A total of 8 sites were included in our registry, with three academic hospitals
355 in each geographic city and five tier-2 district-centered hospitals. In short, our registry covered
356 both tier 3 and tier 2 hospitals with long-term follow-up data. From June 2016 to June 2018, first-
357 time STEMI patients aged ≥ 18 years old who survived at discharge were included. The only
358 exclusion criterion was missing echo data within hospitalization. STEMI was defined as a chest
359 pain lasting ≥ 30 minutes together with an ST-segment elevation in ≥ 2 contiguous leads on a
360 standard 12-lead electrocardiogram (≥ 2 mm in precordial leads and ≥ 1 mm in the limb leads).

361

362 **Mice**

363 Adult C57BL/6N mice were purchased from Shanghai SLAC Laboratory, C57BL/6N *Gsdmd*^{-/-}
364 mice were purchased from GemPharmatech. The knockout of *Gsdmd* gene was validated by
365 genotyping and immunoblotting. All animal surgeries were performed at 10- to 14-week-old male
366 mice. All animals were housed in a pathogen-free environment in the Tongji University animal
367 facilities and all animal experiments were approved by the Tongji University Animal Research
368 Committee (TJLAL-019-128).

369 To deplete neutrophils in mice, isotype IgG (Cell Signalling), anti-Ly6G antibody (BioLegend) or
370 anti-Ly6G/Ly6C antibody (BioLegend) were injected intraperitoneally at a dose of 200 μ g per
371 mouse, as described previously(30, 31). The relevant mice were subjected to myocardial infarction
372 surgery 24 hours later.

373 For NSA administration, 20 mg/ kg mouse weight of NSA (MedChemExpress) was injected
374 intraperitoneally at 30 minutes before AMI surgery, a second injection was given at 8 hours after
375 the surgery. Mice in the corresponding control groups were injected with the same amount of
376 solvent without the chemical compounds.

377

378 **Myocardial infarction**

379 Mice were intubated and ventilated with 1-2% isoflurane. After left thoracotomy, the left coronary
380 artery was ligated with a 6-0 polyester suture 1 mm below the left atrial appendage. Core
381 temperature was monitored and maintained at 37 °C, and the ECG was monitored to document ST-
382 segment elevation during coronary occlusion. Surgeries were performed blinded to the genotypes.
383 At corresponding time points, the mice were euthanized and the samples harvested.

384

385 **Myocardial ischemia reperfusion and 2,3,5- triphenyltetrazolium chloride (TTC) staining**

386 Mice were anesthetized by spontaneous inhalation of isoflurane and maintained under general
387 anesthesia with 1% isoflurane. A left coronary artery occlusion was performed. 30 minutes later,
388 the occlusion was reperused for 24 hours prior to euthanization. The hearts were then harvested,
389 dissected, and stained with Evans blue dye and triphenyltetrazolium chloride. The images were
390 captured under a Leica microscope and the ischemic area at risk and the area of necrosis were
391 quantified. Quantitation of the infarct area was normalized as a percentage of the nonperfused risk
392 area during coronary occlusion.

393

394 **Echocardiography**

395 Echocardiography was performed before the AMI and at 7 days after AMI using a Vevo 2100
396 system (VisualSonics). Mice were kept under light anesthesia, and ultrasound gel was placed in
397 the shaved chest and the probe was adjusted to a stable position. Midventricular M-mode
398 echocardiogram was acquired at the level of the papillary muscles. Heart rate, intraventricular
399 septum and posterior wall thickness, and end-diastolic and end-systolic internal dimensions of the
400 left ventricle were obtained from the M-mode image.

401

402 **Protein analysis by immunoblotting or ELISA**

403 For heart tissues samples, hearts were harvested from mice, rinsed with cold PBS, and divided into
404 left ventricle and right ventricle. The tissues were immediately frozen in liquid nitrogen and then
405 transferred to -80 °C before homogenization. Total protein from tissues or cells was extracted in
406 RIPA buffer (Cell Signaling) supplemented with protease and phosphatase inhibitor cocktail
407 (Roche). Total protein concentration was determined by BCA assay (Pierce). Protein was
408 denatured by mixing with LDS sample buffer (GenScript) and β -ME (Amresco) and heating. Equal
409 amounts of protein were loaded to SurePAGE gels (GenScript) and subjected to gel electrophoresis,
410 followed by blotting onto PVDF membranes (Millipore). Western blotting analysis was performed
411 using antibodies against GSDMD (Abcam), NLRP3 (Cell Signaling), Caspase-1 (Adipogen), IL-
412 1β (R&D Systems), HSP90 (Cell Signaling) and β -tubulin (Cell Signaling) followed by HRP-
413 conjugated secondary antibodies (Invitrogen). The blot was visualized with SuperSignal West
414 Femto substrate (Pierce) on a ChemiDoc Imaging System (Bio-Rad) and analyzed in ImageJ. To
415 test secretion levels of IL- 1β and MCP-1 from leukocytes in the infarcted heart, hearts were

416 harvested, rinsed in cold PBS and minced into small pieces, single cell suspensions were prepared
417 and myeloid-originated cells were isolated using a CD11b antibody and a cell isolation kit in LS
418 Column (Miltenyi Biotech) according to the manufacturer's instructions. The isolated myeloid-
419 originated cells were then counted and cell numbers were adjusted to a same level, the cells were
420 cultured for 24 hours, the supernatant was harvested, purified by centrifugation and further tested
421 in ELISA assays. The cell supernatant was tested for IL-1 β levels by Mouse IL-1 beta/IL-1F2
422 Quantikine ELISA Kit (R&D Systems) and lactate dehydrogenase (LDH) levels by CytoTox 96®
423 Non-Radioactive Cytotoxicity Assay (Promega) according to the manufacturer's instructions. To
424 test IL-1 β or LDH levels in the serum, blood was drawn from the apex of heart, rested in a
425 microcentrifuge tube for 30 minutes, and centrifuged at 1,500 g for 15 minutes, the supernatant
426 serum was aliquoted and stored at -80 °C till the test.

427

428 **Bone-marrow transplantation (BMT)**

429 The recipient mice were given acidic water (pH 2.6) supplemented with neomycin and polymyxin
430 B (both from BBI) 1 week prior to irradiation. The irradiation was given by a small animal X-ray
431 irradiator (Rad Source) at a dose of 8 Gy. The donor bone marrow cells were isolated from the
432 femurs of donor mice and injected into the recipient mice by tail vein injection within 4 hours after
433 the irradiation (at a cell number of 5×10^6 per mouse). The recipient mice were housed for 4 more
434 weeks prior to myocardial infarction surgery. Spleen tissues were harvested and immunoblotting
435 was performed to confirm that the bone marrow cells had been replaced.

436

437 **Immunofluorescence, TUNEL and Masson's trichrome staining**

438 The hearts were harvested from euthanized mice, perfused from the apex with cold PBS to remove
439 contaminating blood, embedded in OCT (Sakura) and then flash frozen. 5 μm frozen sections from
440 mouse hearts were prepared for immunofluorescence staining. The sections were fixed with 4%
441 paraformaldehyde for 30 minutes and washed in PBS, antigen retrieval was performed by boiling
442 the sections in sodium citrate. The sections were then permeabilized in 1% Triton X-100 (Sigma
443 Aldrich) for 10 minutes and blocked in 1% BSA for 30 minutes. Primary antibodies were diluted
444 in 1% BSA and the sections were incubated with antibody dilutions at 4 $^{\circ}\text{C}$ overnight. The sections
445 were then washed in PBS, incubated with secondary antibody dilutions and washed in PBS again.
446 Subsequently, the sections were stained with DAPI (Invitrogen) and mounted with Prolong Gold
447 Antifade Mountant (Invitrogen). The slides were scanned by a Nikon confocal microscope and
448 quantification was performed in ImageJ. The immunofluorescence staining was performed using
449 antibodies against CD68 (Abcam), MPO (R&D Systems) and alpha Actinin (Abcam). For TUNEL
450 staining, 5 μm frozen sections were stained using a *In Situ* Cell Death Detection Kit (Roche)
451 according to the manufacturer's instructions. For Masson's trichrome staining, 10 μm frozen
452 sections from mouse hearts were prepared, the sections were stained with a Masson's Trichrome
453 kit (Nanjing Jiancheng Bioengineering Institute) according to the manufacturer's instructions. The
454 images were captured by a Leica microscope and the images of 7 sections were used for the
455 quantification of fibrotic area and ventricular wall thickness.

456

457 **Flow cytometry**

458 Leukocytes from blood, bone marrow and heart were applied to flow cytometric analysis. Blood
459 was drawn directly from the apex into centrifuge tubes containing 3.8% sodium citrate. The red

460 blood cells were lysed by RBC lysis buffer (BioLegend). The cells were centrifuged at 2,000 rpm
461 for 3 minutes at 4 °C and the cell pellets were resuspended in antibody dilutions. To isolate
462 leukocytes from bone marrow, femurs from mice were isolated, cleaned and the ends were cut
463 open by a scissor. The bone marrow was flushed with cold PBS using a 23-gauge needle, filtered
464 through a 100 µM strainer and centrifuged at 2,000 rpm for 3 minutes at 4 °C. The supernatant
465 was discarded, the red blood cells were removed by RBC lysis buffer, and the cells were washed
466 before resuspension in antibody dilutions. To analyze leukocytes in the heart, single cell
467 suspensions were initially prepared. Hearts were harvested, rinsed with cold PBS, and minced into
468 pieces. The tissues were incubated in a cocktail of collagenase I (450 U/ml), collagenase XI (125
469 U/ml), hyaluronidase type I-s (60 U/ml) and DNase (60 U/ml) (all from Sigma-Aldrich) at 37 °C
470 for 1 hour with gentle agitation. After digestion, the single cell suspensions were then filtered
471 through a 100 µM strainer into a 50 mL tube, rinsed with FACS buffer and centrifuged at 2,000
472 rpm for 3 minutes. The cell pellets were resuspended in antibody dilutions and incubated at room
473 temperature for 30 minutes in dark. The following antibodies have been used: CD45-BV605,
474 CD11b-AlexaFluor647, Ly6G-FITC, Ly6C-Perp-cy5.5 (all from BioLegend). Data was acquired
475 on a LSRFortessa flow cytometer (BD Biosciences) and analyzed in FlowJo (Version 10.6.2). The
476 the myeloid leukocytes were identified as CD45⁺CD11b⁺ and further classified as Ly6G positive
477 neutrophils, Ly6C positive monocytes.

478 **Myeloid-derived cells and Neutrophils Isolation and Culture**

479 In order to explore the function of myeloid-derived cells and neutrophils, we isolated neutrophils
480 in the heart by using the CD11b MicroBeads UltraPure or the neutrophil separation kit (Miltenyi
481 Biotec) according to the manufacturer's instructions, as described previously (32). Myeloid-
482 derived cells and neutrophils were isolated from the heart of mice with different time points post

483 myocardial infarction, followed by immunoblotting or ELISA. The viability of the neutrophils
484 cultured for 24 and 72 hours was determined with an annexin V/PI staining kit (Thermo Fisher
485 Scientific), followed by flow cytometry as described previously (33, 34).

486 **RNA-seq data processing**

487 Total RNAs derived from whole heart post AMI (Day 1), AMI (Day 7) and Sham were applied for
488 whole transcriptome sequencing. Briefly, cDNA library was prepared using random hexamer
489 primer and PCR amplification. PCR products were purified (AMPure XP system) and library
490 quality was assessed on the Agilent Bioanalyzer 2100 system. After cluster generation via using
491 TruSeq PE Cluster Kit v3-cBot-HS (Illumina), the library preparations were sequenced on an
492 Illumina HiSeq platform and 150 bp paired-end reads were generated.

493 The quality of the reads was evaluated with FastQC. The reads were then trimmed with Cutadapt
494 to remove low quality bases and remove adapters. Alignment of the resulting high-quality reads to
495 the mouse reference Ensembl Version GRCh38.92 was performed via the splice-aware aligner
496 STAR (v2.4.0j). Afterwards, using RSEM (RNA-Seq by Expectation Maximization), the
497 abundance of each gene was quantified as TPM (Transcripts per million) value. All original data
498 were deposited in the NCBI's Gene Expression Omnibus database (GEO GSE181872).

499

500 **Principal component analysis**

501 We calculated the standard deviation (SD) of each gene across samples and selected those with
502 $SD \geq 0.5$ to generate 1st and 2nd principal component with the unsupervised learning technique,
503 Principal Component Analysis (PCA).

504

505 **Analysis of differentially expressed genes (DEGs)**

506 The DEGs, defined by fold change (FC) ≥ 2 and a false discovery rate (FDR) < 0.05 , was called
507 using the DESeq2, and were used to generate a hierarchical clustering with the “pheatmap”
508 package in R. The intersections of DEGs created from different comparisons were calculated via
509 the “VennDiagram” package. DEGs that had coherent expression patterns across Sham, AMI (Day
510 1) and AMI (Day 7) were further clustered together. The genes in different patterns were
511 respectively mapped onto the Gene Ontology (GO), and the adjusted p value indicating whether a
512 function was enriched by DEGs was calculated using the hypergeometric distribution.

513

514 **Statistics**

515 All data were presented as mean \pm SD. Comparison of two groups were performed by an unpaired
516 two-tailed Student’s *t* test. When more than two groups were compared, statistical significance
517 was determined using One-way analysis of variance followed by Tukey’s multiple comparison test
518 or Bonferroni’s multiple comparison test. A difference of $P < 0.05$ was considered as significant
519 and labeled with one star, a difference of $P < 0.01$ was labeled with two stars, a difference of $P <$
520 0.001 was labeled with three stars, a difference of $P < 0.0001$ was labeled with four stars.
521 Statistical significances of Kaplan-Meier survival curves were determined by Mantel-Cox test.
522 Relationships between variables were determined by the Pearson correlation coefficient. The
523 statistical analysis was performed with Prism (GraphPad Software, version 8.3.0).

524

525 **Study approval**

526 For animal studies, all animal experiments were approved by the Tongji University Animal
527 Research Committee (TJLAL-019-128). For human studies, it was approved centrally by the
528 Ethics Committee at Shanghai Chest Hospital, Shanghai Jiaotong University (approved number
529 2015-111) and by the local health research ethics board at each participating hospital. Written
530 informed consent was obtained from each patient to allow for follow-up data.

531

532 **Author contributions:**

533 Y. Xiang designed the study; K.J., Z.T., K.C., F.C, S.X, T.S and D.W. performed the animal
534 experiments and the in vitro experiments; Y. Xiang, K.C., K.J, Y. Xu, J.Q, L.S and J.H analyzed
535 the data. Y. Xiang wrote the manuscripts. K.J., Z.T., and K.C. are co–first authors based on their
536 distinct contributions; the order of co–first authors was determined based on the overall scientific
537 contribution.

538

539 **Acknowledgments:**

540 Y. Xiang received support from the National Outstanding Youth Science Fund Project of National
541 Natural Science Foundation of China (81822048), the National Key Research and Development
542 Program of China (2017YFC1700402), Fundamental Research Funds for the Central Universities
543 (22120200064), and the Frontier Science Research Center for Stem Cells, Ministry of Education.
544 We acknowledge Dr. Jiandong Liu for helpful discussions and advice.

545 **Conflict of interest:** none declared.

546 **References**

- 547 1. Heusch G. Myocardial ischaemia-reperfusion injury and cardioprotection in perspective.
548 *Nat Rev Cardiol.* 2020;17(12):773-89.
- 549 2. Lavandero S, Chiong M, Rothermel BA, and Hill JA. Autophagy in cardiovascular
550 biology. *J Clin Invest.* 2015;125(1):55-64.
- 551 3. Prabhu SD, and Frangogiannis NG. The Biological Basis for Cardiac Repair After
552 Myocardial Infarction: From Inflammation to Fibrosis. *Circ Res.* 2016;119(1):91-112.
- 553 4. Rock KL, and Kono H. The inflammatory response to cell death. *Annu Rev Pathol.*
554 2008;3(99-126).
- 555 5. Ong SB, Hernandez-Resendiz S, Crespo-Avilan GE, Mukhametshina RT, Kwek XY,
556 Cabrera-Fuentes HA, and Hausenloy DJ. Inflammation following acute myocardial
557 infarction: Multiple players, dynamic roles, and novel therapeutic opportunities.
558 *Pharmacol Ther.* 2018;186(73-87).
- 559 6. Seropian IM, Toldo S, Van Tassell BW, and Abbate A. Anti-inflammatory strategies for
560 ventricular remodeling following ST-segment elevation acute myocardial infarction. *J*
561 *Am Coll Cardiol.* 2014;63(16):1593-603.
- 562 7. Abbate A, Toldo S, Marchetti C, Kron J, Van Tassell BW, and Dinarello CA. Interleukin-
563 1 and the Inflammasome as Therapeutic Targets in Cardiovascular Disease. *Circ Res.*
564 2020;126(9):1260-80.
- 565 8. Toldo S, and Abbate A. The NLRP3 inflammasome in acute myocardial infarction. *Nat*
566 *Rev Cardiol.* 2018;15(4):203-14.
- 567 9. van Hout GP, Bosch L, Ellenbroek GH, de Haan JJ, van Solinge WW, Cooper MA,
568 Arslan F, de Jager SC, Robertson AA, Pasterkamp G, et al. The selective NLRP3-
569 inflammasome inhibitor MCC950 reduces infarct size and preserves cardiac function in a
570 pig model of myocardial infarction. *Eur Heart J.* 2017;38(11):828-36.
- 571 10. Kawaguchi M, Takahashi M, Hata T, Kashima Y, Usui F, Morimoto H, Izawa A,
572 Takahashi Y, Masumoto J, Koyama J, et al. Inflammasome activation of cardiac
573 fibroblasts is essential for myocardial ischemia/reperfusion injury. *Circulation.*
574 2011;123(6):594-604.
- 575 11. Sager HB, Heidt T, Hulsmans M, Dutta P, Courties G, Sebas M, Wojtkiewicz GR, Tricot
576 B, Iwamoto Y, Sun Y, et al. Targeting Interleukin-1beta Reduces Leukocyte Production
577 After Acute Myocardial Infarction. *Circulation.* 2015;132(20):1880-90.
- 578 12. Liu X, Zhang Z, Ruan J, Pan Y, Magupalli VG, Wu H, and Lieberman J. Inflammasome-
579 activated gasdermin D causes pyroptosis by forming membrane pores. *Nature.*
580 2016;535(7610):153-8.
- 581 13. Shi J, Zhao Y, Wang K, Shi X, Wang Y, Huang H, Zhuang Y, Cai T, Wang F, and Shao
582 F. Cleavage of GSDMD by inflammatory caspases determines pyroptotic cell death.
583 *Nature.* 2015;526(7575):660-5.
- 584 14. Ruhl S, Shkarina K, Demarco B, Heilig R, Santos JC, and Broz P. ESCRT-dependent
585 membrane repair negatively regulates pyroptosis downstream of GSDMD activation.
586 *Science.* 2018;362(6417):956-60.
- 587 15. Broz P, Pelegrin P, and Shao F. The gasdermins, a protein family executing cell death
588 and inflammation. *Nat Rev Immunol.* 2020;20(3):143-57.
- 589 16. Sreejit G, Abdel-Latif A, Athmanathan B, Annabathula R, Dhyani A, Noothi SK, Quaiife-
590 Ryan GA, Al-Sharea A, Pernes G, Dragoljevic D, et al. Neutrophil-Derived S100A8/A9
591 Amplify Granulopoiesis After Myocardial Infarction. *Circulation.* 2020;141(13):1080-
592 94.

- 593 17. Chen KW, Demarco B, Ramos S, Heilig R, Goris M, Grayczyk JP, Assenmacher CA,
594 Radaelli E, Joannas LD, Henao-Mejia J, et al. RIPK1 activates distinct gasdermins in
595 macrophages and neutrophils upon pathogen blockade of innate immune signaling. *Proc*
596 *Natl Acad Sci U S A*. 2021;118(28).
- 597 18. Karmakar M, Minns M, Greenberg EN, Diaz-Aponte J, Pestonjamas K, Johnson JL,
598 Rathkey JK, Abbott DW, Wang K, Shao F, et al. N-GSDMD trafficking to neutrophil
599 organelles facilitates IL-1beta release independently of plasma membrane pores and
600 pyroptosis. *Nat Commun*. 2020;11(1):2212.
- 601 19. Han X, Wang R, Zhou Y, Fei L, Sun H, Lai S, Saadatpour A, Zhou Z, Chen H, Ye F, et
602 al. Mapping the Mouse Cell Atlas by Microwell-Seq. *Cell*. 2018;172(5):1091-107 e17.
- 603 20. De Schutter E, Roelandt R, Riquet FB, Van Camp G, Wullaert A, and Vandenaabeele P.
604 Punching Holes in Cellular Membranes: Biology and Evolution of Gasdermins. *Trends*
605 *Cell Biol*. 2021;31(6):500-13.
- 606 21. Zhang CJ, Jiang M, Zhou H, Liu W, Wang C, Kang Z, Han B, Zhang Q, Chen X, Xiao J,
607 et al. TLR-stimulated IRAK4 activates caspase-8 inflammasome in microglia and
608 promotes neuroinflammation. *J Clin Invest*. 2018;128(12):5399-412.
- 609 22. Rathkey JK, Zhao J, Liu Z, Chen Y, Yang J, Kondolf HC, Benson BL, Chirieleison SM,
610 Huang AY, Dubyak GR, et al. Chemical disruption of the pyroptotic pore-forming
611 protein gasdermin D inhibits inflammatory cell death and sepsis. *Sci Immunol*.
612 2018;3(26).
- 613 23. Frangogiannis NG. The inflammatory response in myocardial injury, repair, and
614 remodelling. *Nat Rev Cardiol*. 2014;11(5):255-65.
- 615 24. Westman PC, Lipinski MJ, Luger D, Waksman R, Bonow RO, Wu E, and Epstein SE.
616 Inflammation as a Driver of Adverse Left Ventricular Remodeling After Acute
617 Myocardial Infarction. *J Am Coll Cardiol*. 2016;67(17):2050-60.
- 618 25. Mezzaroma E, Toldo S, Farkas D, Seropian IM, Van Tassell BW, Salloum FN, Kannan
619 HR, Menna AC, Voelkel NF, and Abbate A. The inflammasome promotes adverse
620 cardiac remodeling following acute myocardial infarction in the mouse. *Proc Natl Acad*
621 *Sci U S A*. 2011;108(49):19725-30.
- 622 26. Evavold CL, Ruan J, Tan Y, Xia S, Wu H, and Kagan JC. The Pore-Forming Protein
623 Gasdermin D Regulates Interleukin-1 Secretion from Living Macrophages. *Immunity*.
624 2018;48(1):35-44 e6.
- 625 27. Horckmans M, Ring L, Duchene J, Santovito D, Schloss MJ, Drechsler M, Weber C,
626 Soehnlein O, and Steffens S. Neutrophils orchestrate post-myocardial infarction healing
627 by polarizing macrophages towards a reparative phenotype. *Eur Heart J*. 2017;38(3):187-
628 97.
- 629 28. Tsuchiya K, Nakajima S, Hosojima S, Thi Nguyen D, Hattori T, Manh Le T, Hori O,
630 Mahib MR, Yamaguchi Y, Miura M, et al. Caspase-1 initiates apoptosis in the absence of
631 gasdermin D. *Nat Commun*. 2019;10(1):2091.
- 632 29. Taabazuing CY, Okondo MC, and Bachovchin DA. Pyroptosis and Apoptosis Pathways
633 Engage in Bidirectional Crosstalk in Monocytes and Macrophages. *Cell Chem Biol*.
634 2017;24(4):507-14 e4.
- 635 30. Boivin G, Faget J, Ancy PB, Gkasti A, Mussard J, Engblom C, Pfirschke C, Contat C,
636 Pascual J, Vazquez J, et al. Durable and controlled depletion of neutrophils in mice. *Nat*
637 *Commun*. 2020;11(1):2762.

- 638 31. Vafadarnejad E, Rizzo G, Krampert L, Arampatzi P, Arias-Loza AP, Nazzal Y, Rizakou
639 A, Knochenhauer T, Bandi SR, Nugroho VA, et al. Dynamics of Cardiac Neutrophil
640 Diversity in Murine Myocardial Infarction. *Circ Res.* 2020;127(9):e232-e49.
- 641 32. Yee PP, Wei Y, Kim SY, Lu T, Chih SY, Lawson C, Tang M, Liu Z, Anderson B,
642 Thamburaj K, et al. Neutrophil-induced ferroptosis promotes tumor necrosis in
643 glioblastoma progression. *Nat Commun.* 2020;11(1):5424.
- 644 33. Geng S, Zhang Y, Lee C, and Li L. Novel reprogramming of neutrophils modulates
645 inflammation resolution during atherosclerosis. *Sci Adv.* 2019;5(2):eaav2309.
- 646 34. Cui C, Chakraborty K, Tang XA, Zhou G, Schoenfelt KQ, Becker KM, Hoffman A,
647 Chang YF, Blank A, Reardon CA, et al. Neutrophil elastase selectively kills cancer cells
648 and attenuates tumorigenesis. *Cell.* 2021;184(12):3163-77 e21.

649

650

651

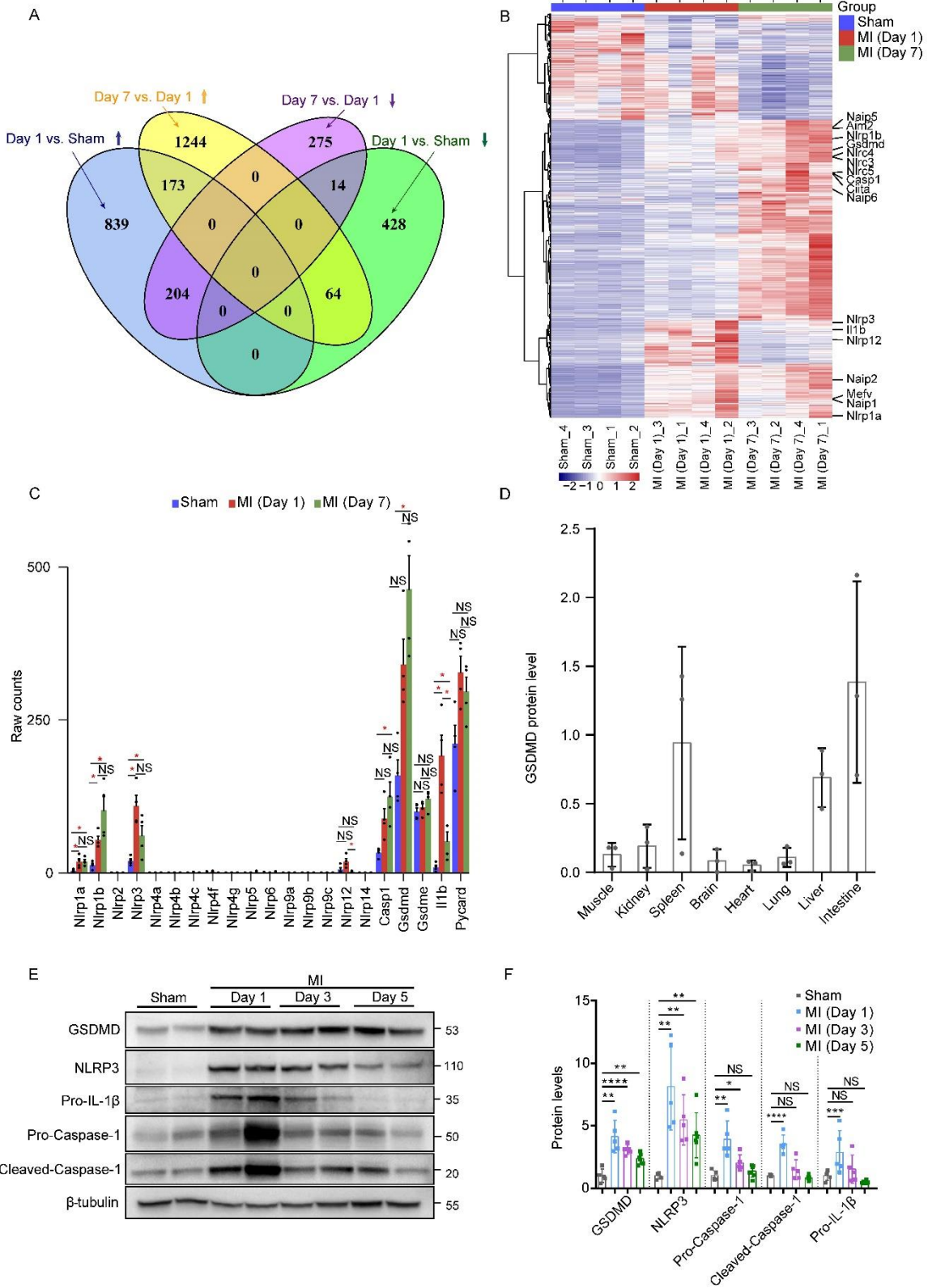
652

653

654

655

Figure 1



657 **Figure 1. GSDMD is activated at the early phase of AMI.**

658 (A) Venn plot revealed the intersection of differentially expressed genes created from the
659 comparisons of MI (Day 1) vs. Sham and MI (Day 7) vs. MI (Day 1). (B) Each row in the heatmap
660 represented a specific gene that had significantly different expression levels in comparisons
661 between any two groups, the expression of which was normalized across the column, with high
662 expression shown in red and low in blue. (C) Bar plot showed the trends of gene expression across
663 Sham, MI (Day 1) and MI (Day 7). * indicated the statistical difference, with fold change (FC) \geq
664 2 and false discovery rate (FDR) < 0.05 . (D) Quantification of GSDMD protein levels by
665 immunoblotting in different tissues of WT (C57BL/6N) mice (n = 3). (E-F) Representative
666 immunoblotting (E) and quantification (F) of left ventricular tissues from mice subjected to MI
667 for different time points (1 day, 3 days, 5 days) or a sham surgery (n = 5 per group), β -tubulin or
668 HSP90 was used as a loading control. Shown are mean \pm SD and were analyzed by One-way
669 analysis of variance with Tukey's correction for multiple comparison (F). NS, not significant; *,
670 $P < 0.05$; **, $P < 0.01$; ***, $P < 0.001$; ****, $P < 0.0001$.

671

672

673

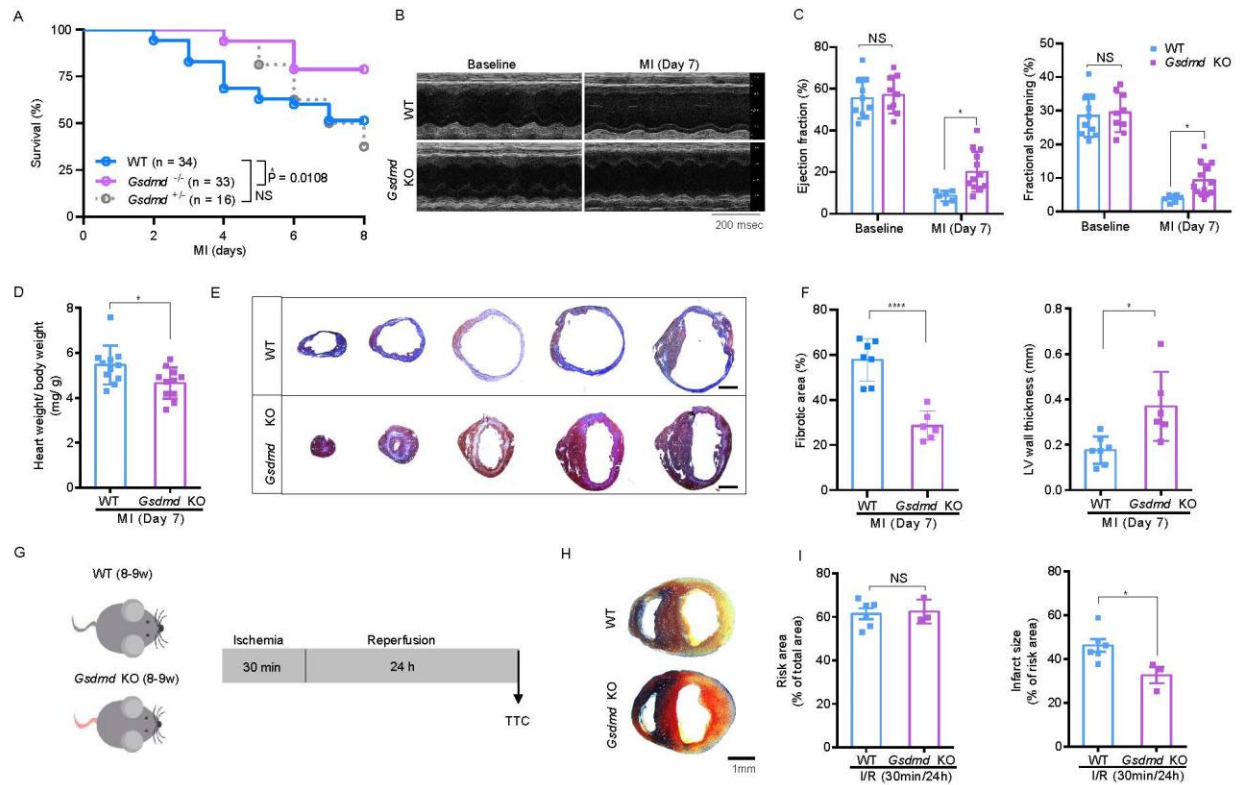
674

675

676

677

Figure 2



678

679 **Figure 2. Loss of GSDMD attenuates myocardial injury post AMI.**

680 (A) Kaplan-Meier survival curves comparing post-MI survival of WT (C57BL/6N) mice (n = 34)
 681 to that of *Gsdmd*^{-/-} mice (n = 33) or *Gsdmd*^{+/-} mice (n = 16). Statistical significance was
 682 determined by Mantel-Cox test. (B-C) Echocardiography images (B) and M-mode quantification
 683 (C) of ejection fraction (left) and fractional shortening (right) for WT or *Gsdmd*^{-/-} mice before or
 684 1 week after MI (baseline: WT, n = 10; *Gsdmd*^{-/-}, n = 9; 1 week: WT, n = 6; *Gsdmd*^{-/-}, n = 12).
 685 (D) A comparison of heart weight/ body weight ratio between WT mice and *Gsdmd*^{-/-} mice 1 week
 686 after MI (WT, n = 11; *Gsdmd*^{-/-}, n = 11). (E-F) Masson's Trichrome staining (E) and quantification
 687 of fibrotic area and left ventricular (LV) wall thickness (F) of short-axis heart sections from WT
 688 or *Gsdmd*^{-/-} mice 1 week after MI (WT, n = 7; *Gsdmd*^{-/-}, n = 6). Scale bar = 1 mm. (G) Schematic

689 diagram showing the ischemia/ reperfusion (I/R) surgery strategy for WT and *Gsdmd*^{-/-} mice. **(H-**
690 **I)** Representative images of Evans blue dye and triphenyltetrazolium chloride (TTC) staining **(H)**
691 and quantification of risk area (left) and infarct size (right) **(I)** for WT or *Gsdmd*^{-/-} mice after I/R
692 surgery (WT, n = 6; KO, n = 3). Statistical tests for **C**: Data represent mean ± SD, NS, not
693 significant; *, *P*<0.05, as analyzed by One-way analysis of variance followed by Bonferroni's
694 multiple comparison test **(C)**. Statistical tests for **D**, **F** and **I**: Data are mean ± SD, NS, not
695 significant; *, *P*<0.05; ****, *P*<0.0001, as analyzed by unpaired two-tailed Student's *t* test.

696

697

698

699

700

701

702

703

704

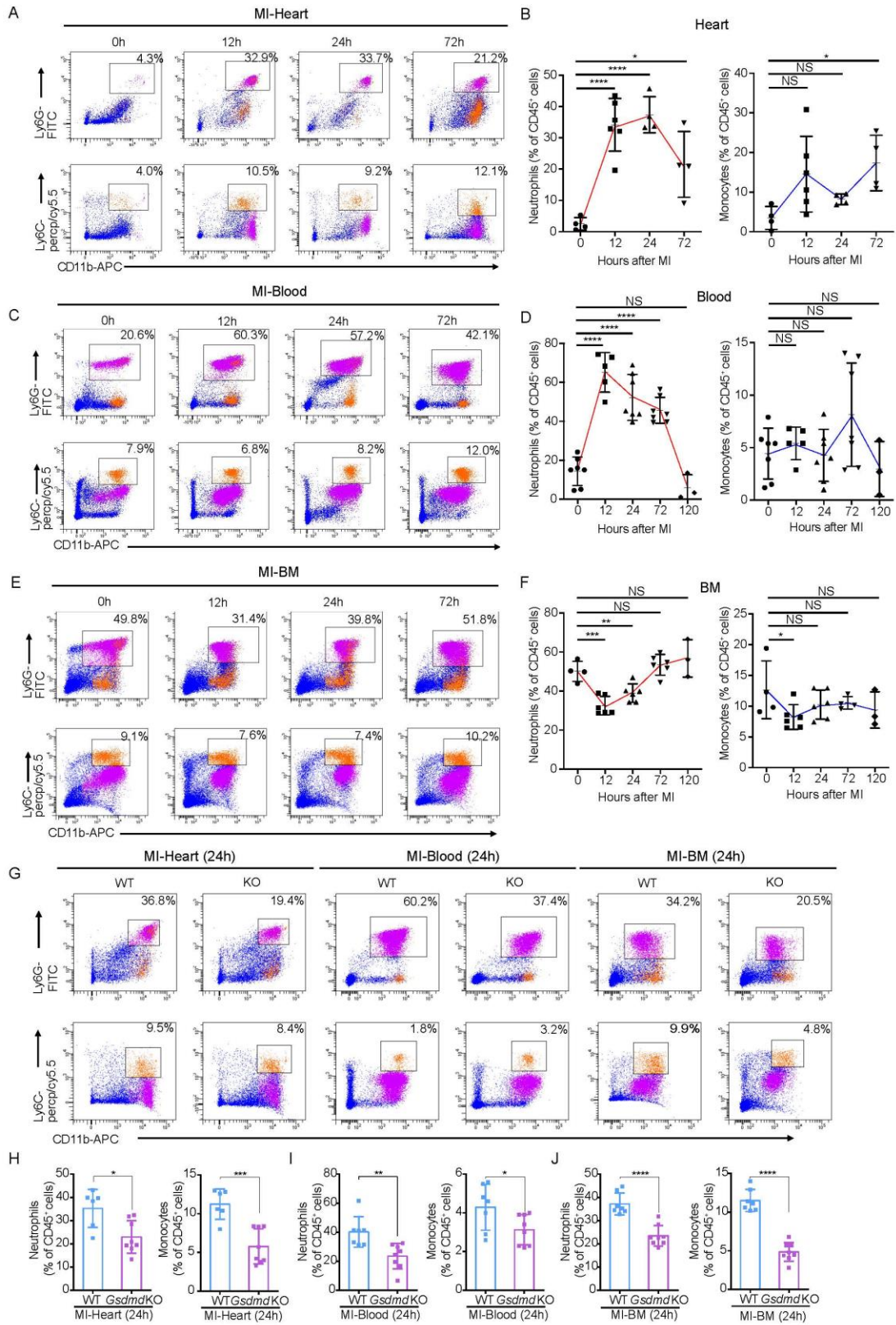
705

706

707

708

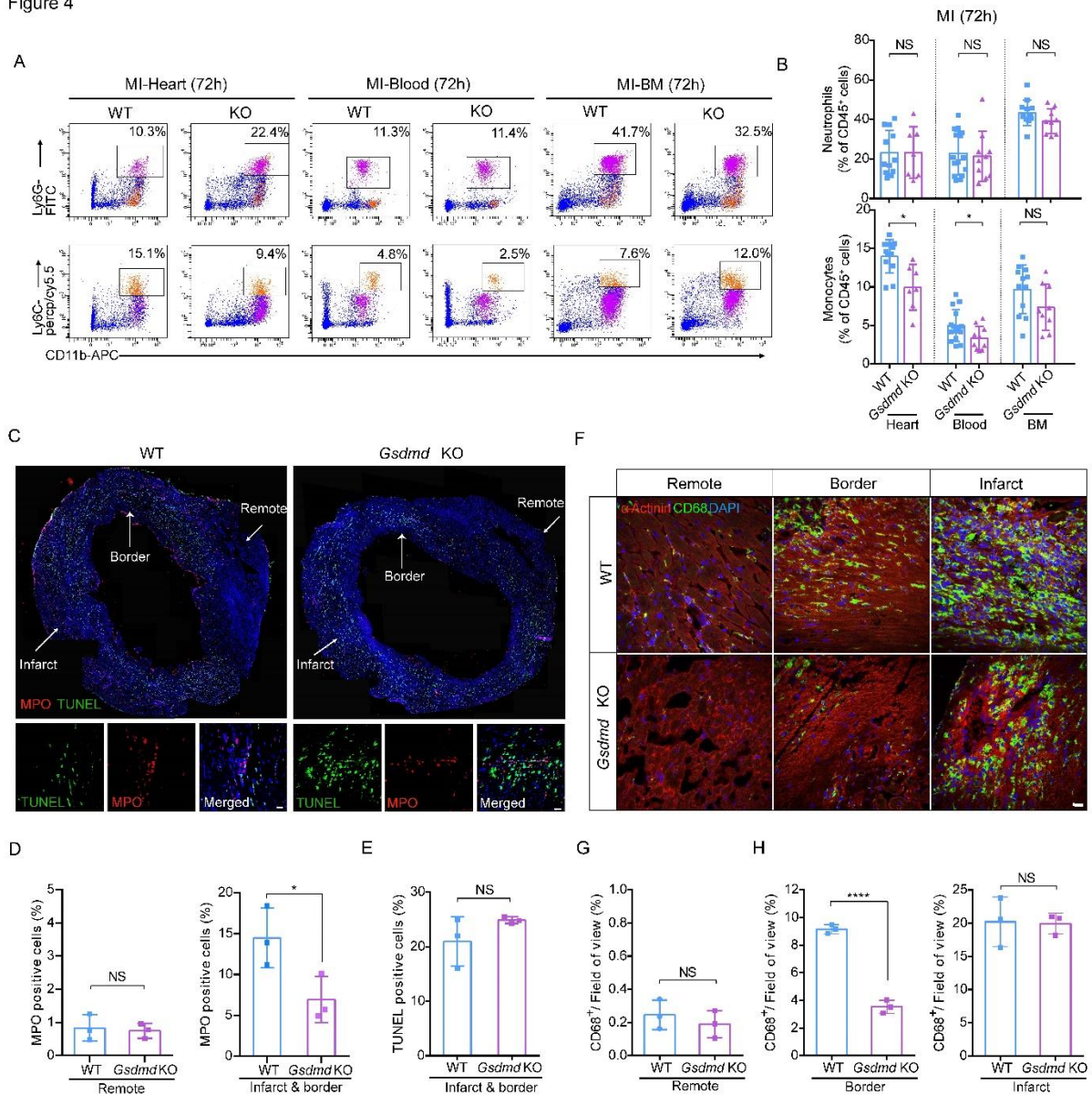
Figure 3



710 **Figure 3. GSDMD is essential for recruitment of neutrophils/monocytes to the AMI heart.**

711 **(A-F)** Flow cytometric analysis and quantification of Cd11b⁺Ly6G⁺ neutrophils and Cd11b⁺Ly6C⁺
712 monocytes in heart **(A)**, blood **(C)** or bone marrow (BM) **(E)** from WT or *Gsdmd*^{-/-} mice at
713 different time points (12 hours, 24 hours, 72 hours) after MI or a sham surgery (n = 4-7), along
714 with their quantification **(B, D and F)**. **(G-J)** Flow cytometric analysis and quantification of
715 Cd11b⁺Ly6G⁺ neutrophils and Cd11b⁺Ly6C⁺ monocytes in heart **(H)**, blood **(I)** or BM **(J)** from
716 WT or *Gsdmd*^{-/-} mice 24 hours after MI (n = 7-8). Data are mean ± SD as analyzed by One-way
717 analysis of variance followed by Bonferroni's multiple comparison test **(B, D and F)** or unpaired
718 two-tailed Student's *t* test **(H, I and J)**. NS, not significant; *, *P*<0.05; **, *P*<0.01; ***, *P*<0.001;
719 ****, *P*<0.0001.

Figure 4



720

721 **Figure 4. GSDMD is essential for recruitment of neutrophils/monocytes to the infarcted**
 722 **heart.**

723 **(A-B)** Flow cytometric analysis and quantification of Cd11b⁺Ly6G⁺ neutrophils and
 724 Cd11b⁺Ly6C⁺ monocytes in heart (left), blood (middle) or BM (right) from WT or *Gsdmd*^{-/-} mice
 725 72 hours after MI (n = 7-15). **(C)** Immunofluorescence imaging and magnification for MPO (red),

726 TUNEL (green) and DAPI (blue) on heart sections from WT or *Gsdmd*^{-/-} mice 24 hours after MI
727 (scale bar, 20 μm). **(D-E)** Quantification of ratios of MPO or TUNEL positive cells of heart
728 sections from WT or *Gsdmd*^{-/-} mice. Each value was averaged from the values of 7 fields of view
729 from the same mouse (n = 3 per group). **(F)** Immunofluorescence imaging on heart sections from
730 WT or *Gsdmd*^{-/-} mice 3 days after MI showing α-Actinin (red), CD68 (green) and DAPI (blue).
731 Representative fields of remote zone, border zone and infarct zone are presented (scale bar, 20
732 μm). **(G-H)** Quantification of CD68 positive area proportion in the field of view in remote zone
733 **(G)**, infarct zone and border zone **(H)** of heart sections from WT or *Gsdmd*^{-/-} mice, each value
734 was averaged from the values of 5 fields of view from the same mouse (n = 3 per group). Statistical
735 tests for **B**: Data represent mean ± SD, NS, not significant; *, *P*<0.05; multiple two-tailed
736 Student's *t* test. Statistical tests for **D, E G and H**: NS, not significant; *, *P*<0.05; ****, *P*<0.0001,
737 unpaired two-tailed Student's *t* test.

738

739

740

741

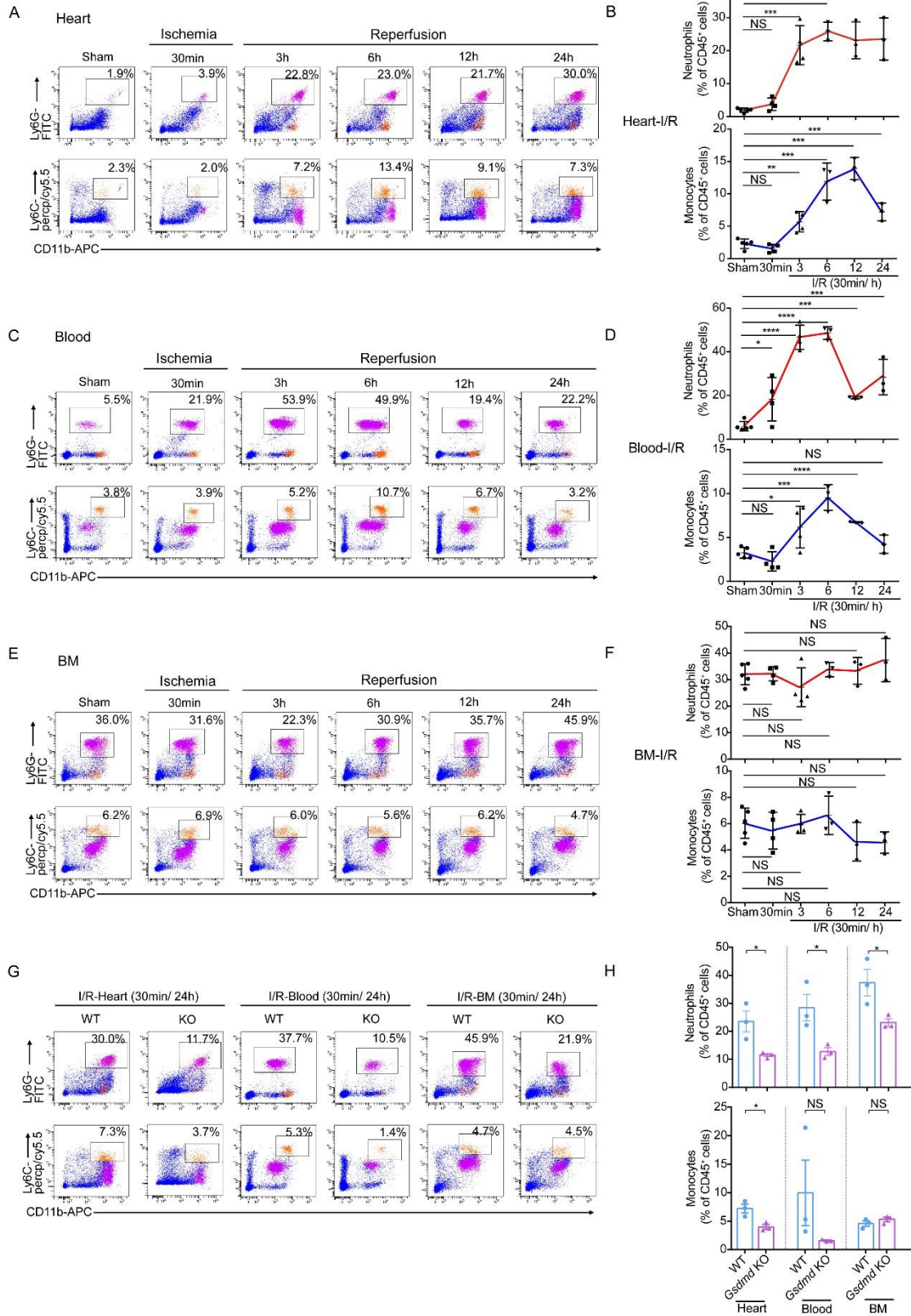
742

743

744

745

Figure 5



747 **Figure 5. GSDMD is essential for recruitment of neutrophils/monocytes to the I/R heart.**
748 **(A-F)** Flow cytometric analysis and quantification of Cd11b⁺Ly6G⁺ neutrophils and Cd11b⁺Ly6C⁺
749 monocytes in heart **(A-B)**, blood **(C-D)** or BM **(E-F)** from WT or *Gsdmd*^{-/-} mice at different
750 reperfusion time points (3 hours, 6 hours, 12 hours, 24 hours) after I/R or a sham surgery.
751 Corresponding n values were indicated in the plots. The statistical significances of sham versus 3h,
752 6h, 12h or 24h were indicated (n = 3-5). **(G-H)** Flow cytometric analysis **(G)** and quantification
753 **(H)** of Cd11b⁺Ly6G⁺ neutrophils and Cd11b⁺Ly6C⁺ monocytes in heart (left), blood (middle) or
754 BM (right) from WT or *Gsdmd*^{-/-} mice 24 hours after I/R (n =3). Data represent mean ±SD, One-
755 way analysis of variance followed by Bonferroni's multiple comparison test **(B, D and F)** or
756 multiple two-tailed Student's *t* test **(H)**. NS, not significant; *, *P*<0.05; **, *P*<0.01; ***, *P*<0.001;
757 ****, *P*<0.0001.

758

759

760

761

762

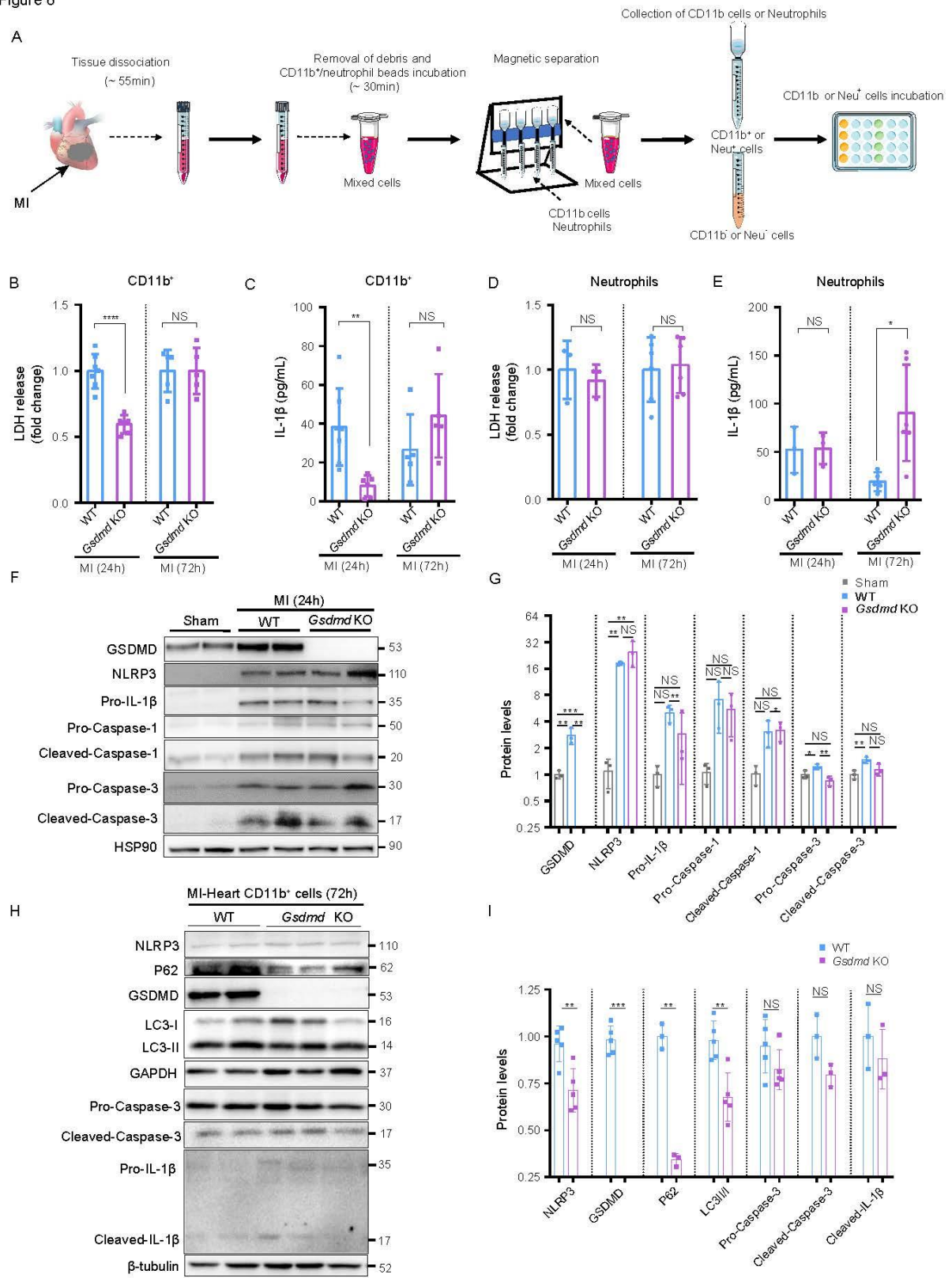
763

764

765

766

Figure 6



768 **Figure 6. GSDMD deficiency suppresses cell death and IL-1 β secretion.**

769 **(A)** Schematic diagram showing the strategy of preparing samples for IL-1 β and lactate
770 dehydrogenase (LDH) detection in Cd11b⁺ myeloid-derived cells and neutrophils from the heart.
771 **(B)** Secretion levels of LDH from leukocytes from the heart of WT or *Gsdmd*^{-/-} mice 24 hours and
772 72 hours after MI. **(C)** Production of IL-1 β from Cd11b⁺ cells from the heart of WT or *Gsdmd*^{-/-}
773 mice 24 hours and 72 hours after MI assessed by ELISA. The corresponding n values were
774 indicated in the plot. **(D)** Secretion levels of LDH from neutrophils isolated from the heart of WT
775 or *Gsdmd*^{-/-} mice 24 hours and 72 hours after MI. **(E)** Production of IL-1 β from neutrophils
776 isolated from the heart of WT or *Gsdmd*^{-/-} mice at 24 hours and 72 hours after MI assessed by
777 ELISA. The corresponding n values were indicated in the plot. **(F-G)** Representative
778 immunoblotting images **(F)** and quantification **(G)** of protein levels in heart left ventricular tissues
779 from WT or *Gsdmd*^{-/-} mice 24 hours after MI or a sham surgery (n = 3 per group) **(H-I)**
780 Representative immunoblotting images **(H)** and quantification **(I)** of protein levels of heart Cd11b⁺
781 cells from WT or *Gsdmd*^{-/-} mice 72 hours after MI or a sham surgery (n = 3-5). Statistical tests
782 for **B-E and I**: Data are mean \pm SD, NS, not significant; *, P<0.05; **, P<0.01;****, P<0.0001,
783 as analyzed by unpaired two-tailed Student's *t* test. Statistical tests for **G**: Data represent mean \pm
784 SD, NS, not significant; *, P<0.05; **, P<0.01; ***, P<0.001, One-way analysis of variance
785 with Tukey's correction for multiple comparison.

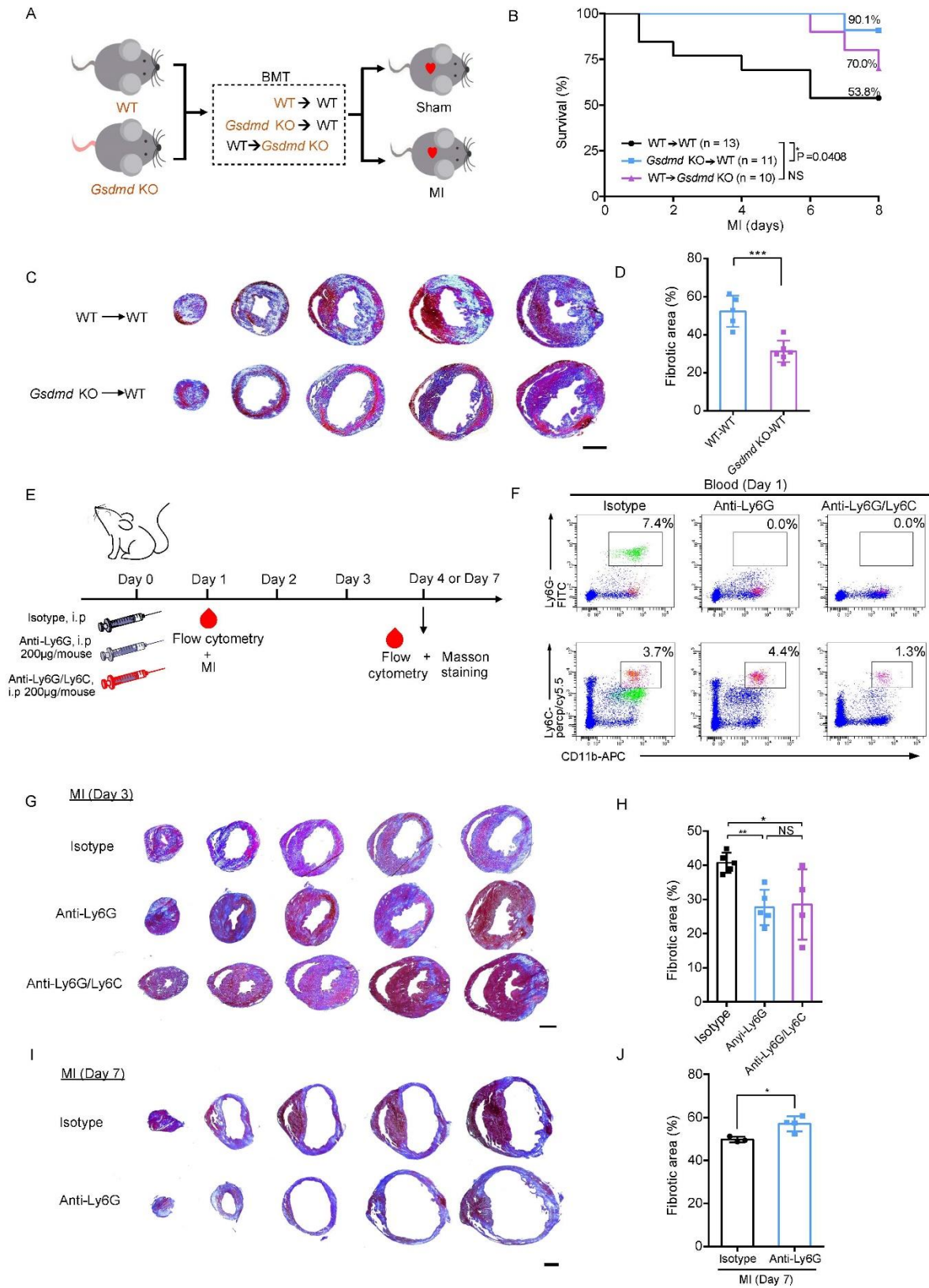
786

787

788

789

Figure 7



791 **Figure 7. GSDMD-dependent bone marrow-derived myeloid cell contributes to acute**
792 **inflammatory response.**

793 **(A)** Schematic diagram showing the strategy of bone marrow transplantation (BMT) experiment.
794 **(B)** Kaplan-Meier survival curves comparing post-MI survival of WT → WT mice (n = 13) to that
795 of *Gsdmd* KO → WT mice (n = 11) or WT → *Gsdmd* KO mice (n = 10). Statistical significance
796 was determined by Mantel-Cox test. **(C-D)** Masson's Trichrome staining **(C)** and quantification
797 **(D)** of fibrotic area of short-axis heart sections from WT → WT (n = 5) or *Gsdmd* KO → WT (n
798 = 6) mice 3 days after MI (scale bar, 1 mm). **(E)** Schematic diagram showing the strategy for
799 neutrophil and monocyte depletion. **(F)** Flow cytometric gating of Ly6G⁺ neutrophils and Ly6C⁺
800 monocytes validating the successful elimination of neutrophils or monocytes in mice. **(G-H)**
801 Masson's Trichrome staining **(G)** and quantification **(H)** of fibrotic area of short-axis heart sections
802 from mice treated with isotype IgG (n = 5), anti-Ly6G antibody (n = 5) or anti-Ly6G/Ly6C
803 antibody (n = 4) 3 days after MI (scale bar, 1 mm). **(I-J)** Masson's Trichrome staining **(I)** and
804 quantification **(J)** of fibrotic area of short-axis heart sections from mice treated with isotype IgG
805 (n = 3), anti-Ly6G antibody (n = 4) 1 week after MI (scale bar, 1 mm). Statistical tests: Data
806 represent mean ±SD and were analyzed by unpaired two-tailed Student's *t* test **(D and J)** or One-
807 way analysis of variance followed by Tukey's multiple comparison test **(H)**. NS, not significant;
808 *, *P*<0.05; **, *P*<0.01; ***, *P*<0.001.

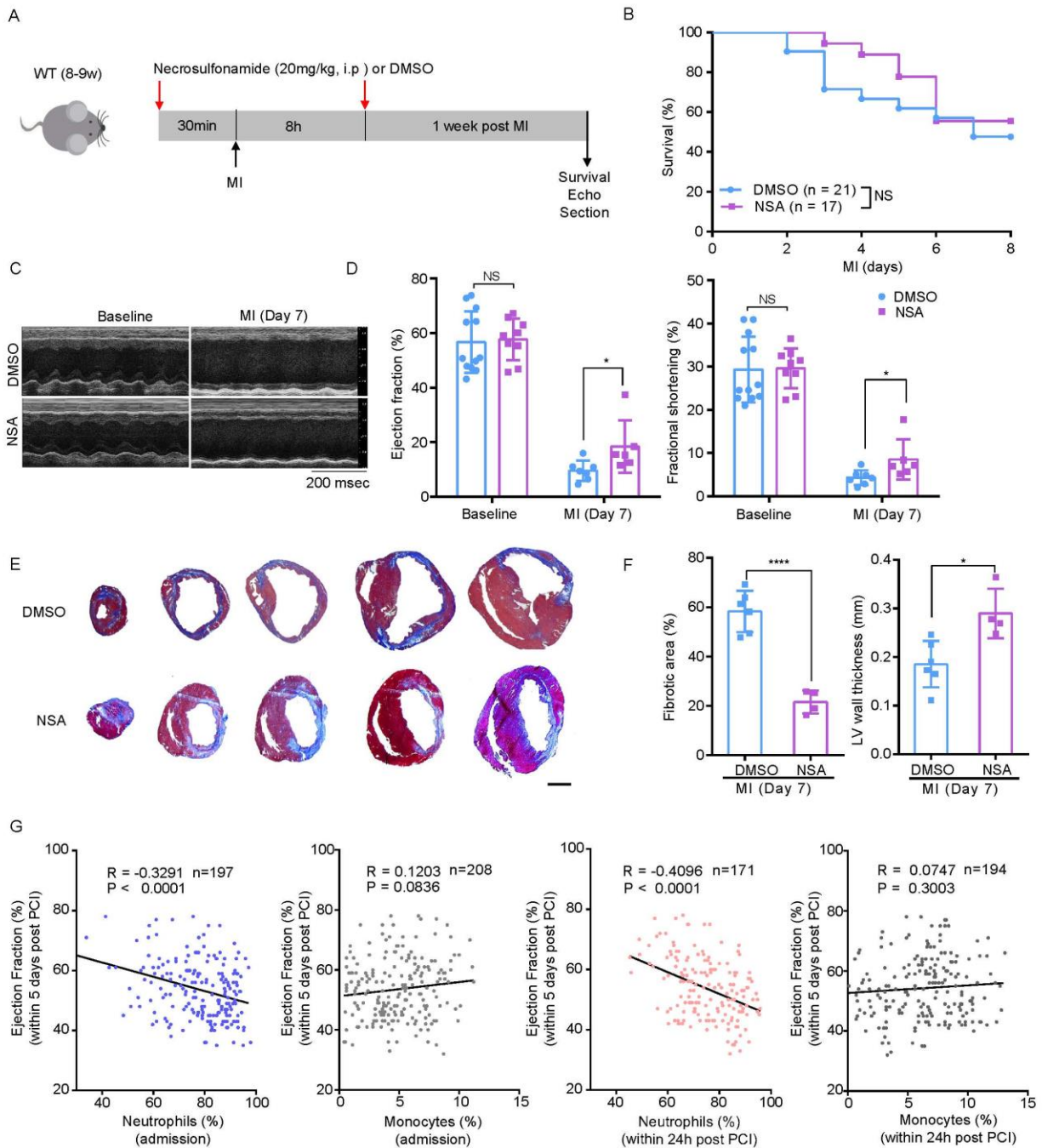
809

810

811

812

Figure 8



813

814 **Figure 8. Pharmacological inhibition of GSDMD reduces infarct size post MI.**

815 **(A)** Schematic diagram showing the strategy of NSA administration to the mice. **(B)** Kaplan-Meier

816 survival curves comparing post-MI survival of control (DMSO administration) mice (n = 21) to

817 that of mice administrated with NSA (n = 17). Significance was determined by Mantel-Cox test.
818 **(C-D)** Echocardiography images **(C)** and M-mode quantification **(D)** of ejection fraction (left) and
819 fractional shortening (right) for control mice or mice with NSA administration before or 1 week
820 after MI. (baseline: DMSO, n = 12; NSA, n= 9; 1 week: DMSO, n = 7; NSA, n = 6). **(E-F)** Masson's
821 Trichrome staining **(E)** and quantification of fibrotic area and left ventricular (LV) wall thickness
822 **(F)** of short-axis heart sections from control mice or mice with NSA administration 1 week after
823 MI (DMSO, n = 6; NSA, n = 4) (scale bar, 1 mm). **(G)** Analysis of correlation between MI patients
824 within 5 days post PCI ejection fraction (EF) and the percentage of neutrophils or monocytes in
825 peripheral blood at the point of the admission or the patients within 24 h post PCI were performed
826 with Pearson's correlation test. Statistical tests: Data represent mean \pm SD and were analyzed by
827 One-way analysis of variance with Tukey's correction for multiple comparison **(D)** or unpaired
828 two-tailed Student's *t* test **(F)**. NS, not significant; *, $P<0.05$; ****, $P<0.0001$.

829

830

831